communications biology

Article

https://doi.org/10.1038/s42003-024-06627-2

The early communication stages between serine proteases and enterovirus capsids in the race for viral disintegration

Check for updates

Marie-Hélène Corre[1] ✉, Benjamin Rey[1], Shannon C. David[1], Shotaro Torii[1], Diego Chiappe[2] & Tamar Kohn[1]

Serine proteases are important environmental contributors of enterovirus biocontrol. However, the structural features of molecular interaction accounting for the susceptibility of enteroviruses to proteases remains unexplained. Here, we describe the molecular mechanisms involved in the recruitment of serine proteases to viral capsids. Among the virus types used, coxsackievirus A9 (CVA9), but not CVB5 and echovirus 11 (E11), was inactivated by Subtilisin A in a host-independent manner, while Bovine Pancreatic Trypsin (BPT) only reduced CVA9 infectivity in a host-dependent manner. Predictive interaction models of each protease with capsid protomers indicate the main targets as internal disordered protein (IDP) segments exposed either on the 5-fold vertex (DE loop VP1) or at the 5/2-fold intersection (C-terminal end VP1) of viral capsids. We further show that a functional binding protease/capsid depends on both the strength and the evolution over time of protease-VP1 complexes, and lastly on the local adaptation of proteases on surrounding viral regions. Finally, we predicted three residues on CVA9 capsid that trigger cleavage by Subtilisin A, one of which may act as a sensor residue contributing to enzyme recognition on the DE loop. Overall, this study describes an important biological mechanism involved in enteroviruses biocontrol.

Enteroviruses are human pathogens known to challenge water safety[1,2]. Among the microbial stressors found in freshwater, bacterial serine proteases contribute to the control of enterovirus persistence[3]. However, not all virus types are equally susceptible to these enzymes and the range of specificity of serine proteases does not solely explain virus inactivation[4]. Accordingly, we performed a functional and model-based predictive structural study of the interaction between enterovirus capsids (CVA9, CVB5 and E11) and serine proteases (Subtilisin A from *Bacillus licheniformis*, Trypsin from bovine pancreas (BPT)), to unravel the molecular steps leading to viral inactivation.

As first partner of interaction, Enterovirus capsids are giant ~5500-kilodalton (kDa) rounded substrates, composed of 60 repeating units of the four viral proteins VP1, VP2, VP3 (protomer) and VP4 (Fig. S1a)[5–7]. The overall capsid architecture is built by the association of 12 repeats of five protomers (12 pentamers), tightly bound together to form an icosahedral shell with a 5:3:2 rotational symmetry (Fig. S1a, b)[5,6,8]. From this structural arrangement, VP1, VP2, VP3 cover the outer lattice and share a similar jelly roll β-sandwich fold, while the minor protein VP4 is plated to the inner surface of the capsid (Fig. S1a–e)[5,6,9]. The eight β-sheets of each jelly roll fold, conventionally designated by the letters B to I, are linked to each other by internal disordered protein (IDP) loops, some of them contributing greatly to the plasticity of both the 5-fold vertex ("mesa") and the 3-fold proper-like protrusion of the capsid (Fig. S1d, e)[10,11]. While *Enterovirus* VP1s share the same core structure, their sequences are known to differ from 279 to 317 amino acids in length depending on virus types[12]. As a result, the C-terminal end of some VP1s (~5 to 20-mer length) is exposed around the 5/2-fold axes intersection of the capsid and constitutes an additional structurally accessible IDP segment[13].

As second partner of interaction, serine proteases are ~25 kDa monomeric enzymes described to catalyze the hydrolysis reaction of peptide bonds under the action of a nucleophilic serine[14]. Trypsins and subtilisins are among the most studied serine proteases and are known to share a similar catalytic pocket geometry[15–19]. The catalytic site of such enzymes is formed by a triad folded structure, which ensures a charge relay between an aspartic acid, a histidine, and the nucleophilic serine[15,18,20]. Moreover, an adjacent residue (glycine or asparagine) is hydrogen bonded to the

[1]Laboratory of Environmental Virology, Environmental Engineering Institute (IIE), School of Architecture, Civil and Environmental Engineering (ENAC), Ecole Polytechnique Fédérale de Lausanne (EPFL), 1015-CH Lausanne, Switzerland. [2]Proteomics Core Facility, School of Life Sciences, Ecole Polytechnique Fédérale de Lausanne (EPFL), 1015-CH Lausanne, Switzerland. ✉e-mail: marie.helene.corre@univ-poitiers.fr

nucleophilic serine, forming an oxyanion hole used to stabilize the reaction intermediate[21,22]. Serine proteases are however distinguished from each other by the specificity of substrate they can hydrolyze. While trypsins specifically hydrolyze the scissile bond following basic amino acids (K, R)[23,24], subtilisins deploy a much broader spectrum of action and tend to include most amino acids as potential substrate, with the exception of asparagine and tryptophane[25–29].

Results

Virus type-specific sensitivity to serine proteases

To investigate the specificity of interaction between capsids and serine proteases leading to virus inactivation, we first selected sensitive and insensitive virus types to Subtilisin A and BPT. As previously described, CVA9 is sensitive to several proteases including BPT and a subtilisin produced by *B. subtilis*[4]. We therefore selected this virus type to set up our antiviral assay with the two proteases. To this end, an environmental CVA9 isolate was exposed for 2 or 6 h to 20 µg/mL of each protease, and the virus' ability to infect Buffalo Green Monkey Kidney (BGMK) cells was measured before and after exposure. The cytopathic effects (CPEs) measured on cells after an exposure with each protease were used to demonstrate the reduction of viral infectivity (Log_{10} C/C_0) (Fig. 1a). Independent of the treatment time, exposure to Subtilisin A led to 1.5 to 3.5-log_{10} reduction of CVA9 infectivity, whereas a similar exposure with BPT reduced viral infectivity by 1.5-log_{10}. With the aim of finding protease-resistant viruses, we reproduced this experiment with the reference strains CVB5 (strain Faulkner) and E11 (strain Gregory), for which sensitivity to these two proteases was unknown. For all experimental conditions, no reduction of the infectivity was observed (Fig. 1b), indicating that the capsid integrity of these two virus types is preserved upon exposure with both proteases.

Protease-specific inactivation of CVA9

Unlike CVB5 and E11, CVA9 exposes on its capsid outer surface a 18-mer hyperflexible C-terminal VP1 sequence (IDP) carrying an RGD motif (Fig. 1c)[13,30,31]. This motif is described to promote CVA9 recognition to BGMK cells through the integrin cell signaling pathway (αVβ3, αVβ6) during the early stages of infection[32–34]. This C-terminal sequence is also known to be a valuable substrate for some proteases, though its cleavage does not influence CVA9 infection via an integrin-independent cellular

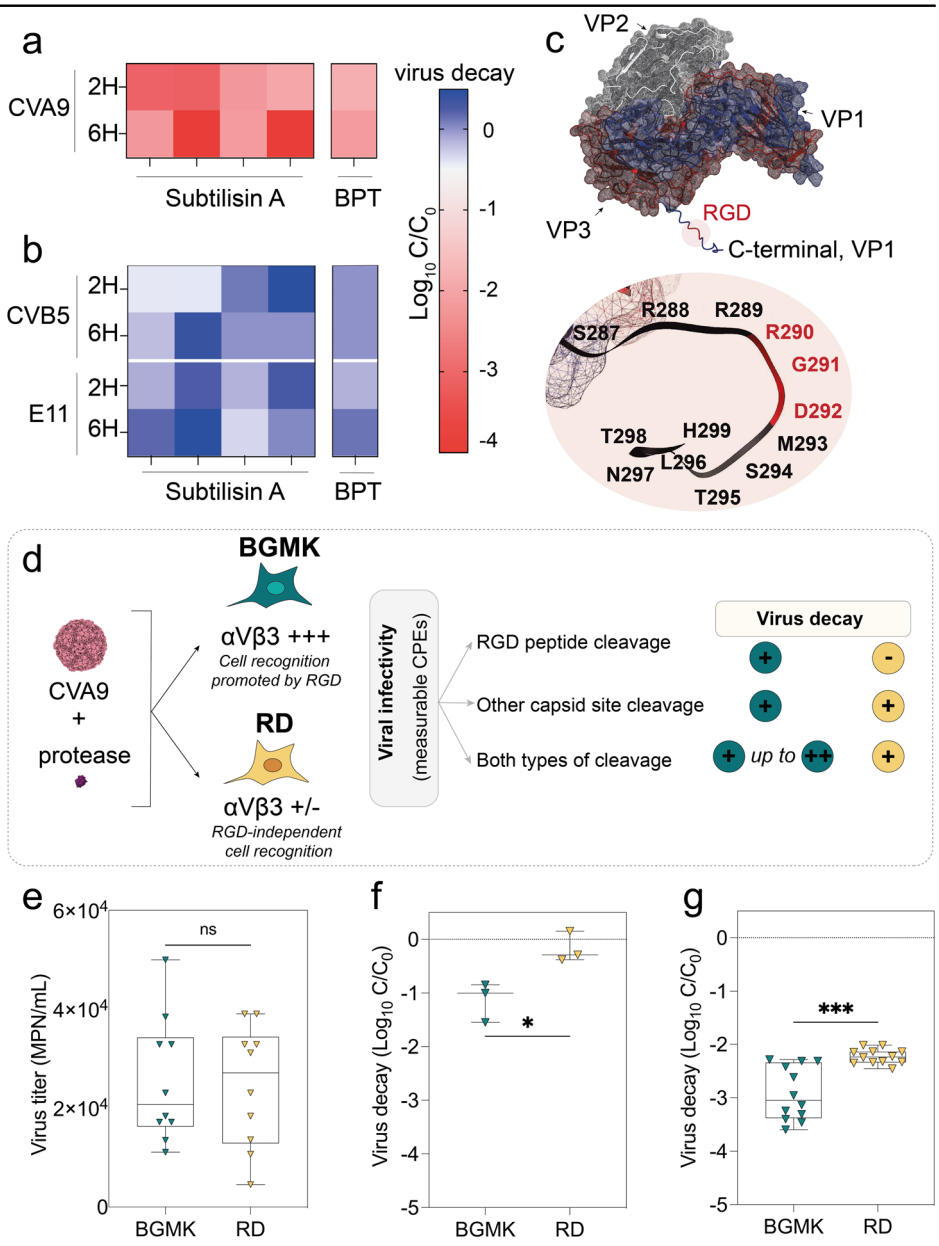

Fig. 1 | Enterovirus inactivation by serine proteases is both virus type and protease specific. Virus decay (Log_{10} C/C_0) of (**a**) CVA9 or (**b**) CVB5 and E11 after an exposure to serine proteases. Each virus has been exposed to 20 µg/mL of Subtilisin A ($n = 4$) or BPT ($n = 1$) for 2 or 6 h. Infectivity experiments have been performed on BGMK cells and cytopathic effects (CPEs) measurements have been done 4-days post-infection. **c** Visualization of the CVA9 C-terminal end VP1 segment (strain Griggs, 1d4m), carrying a RGD motif. Modeling of CVA9 VP1 anchoring the C-terminal end of the protein has been performed using Modeller. **d** Screening procedure used to demonstrate the RGD-independent viral decay of CVA9 by serine proteases. PDB structures used for CVA9 (1d4m) and protease (1scn) visuals. **e** Comparison of CVA9 viral titers 5-days post-infection on BGMK and RD cells ($t = 0.1667$, p value: 0.8695 (ns); two-tailed unpaired t-test, $n = 10$). Comparison of CVA9 viral decay measured on BGMK and RD cells after an exposure either with 20 ug/mL BPT (**f**) ($t = 3.583$, p value: 0.0256 (*); two-tailed unpaired t-test, $n = 3$) or Subtilisin A (**g**) ($t = 4.614$, p value: 0.0005 (***); two-tailed unpaired t-test, $n = 12$) for 2 h. For each experiment involving a treatment with proteases, the LoD of the assay was 5-log_{10}. For all negative control experiments of inactivation (C_0), PBS has been used to replace serine proteases. **e**–**g** For each box plot, the horizontal bar within the interquartile range corresponds to the median of values. The vertical bar of each dataset corresponds to the distribution of minimum and maximum values.

bypass process[35,36]. To investigate whether Subtilisin A and BPT attack this IDP on CVA9 capsid, we developed a differential cell culture approach based on integrins recognition (Fig. 1d). We exposed CVA9 to each protease, before measuring its infectivity on both BGMK cells (RGD-promoted cell recognition) and human Rhabdomyosarcoma (RD) cells, known to be permissive to CVA9 in an RGD-independent manner[36,37]. Prior to this experiment, the percentage of cells expressing each integrin type (i.e., αVβ3, αVβ6) was assessed by flow cytometry for both cell lines (Fig. S2a, b). We counted on average 9.5-fold more αVβ3-type integrin on the surface of BGMK cells (40–90% positive cells) than on RD cells (1–6% positive cells), whereas αVβ6-type integrin expression was similar for both cell lines (5% positive cells). We then monitored the CPEs induced by CVA9 on RD and BGMK cells to standardize our viral assay and to further study the C-terminal end sequence cleavage by serine proteases (Fig. S2c). Similar viral titers were measured on both cell lines 5-days post-infection (~$0.5.10^5$ MPN/mL, p value = 0.8695, unpaired t-test) (Fig. 1e), confirming that neither random nor cell-line-specific factors (i.e. integrins proportion, other attachment proteins, protein from media) influenced the infectivity of CVA9 on either cell lines. We then applied the same protocol after an exposure of CVA9 virions to 20 µg/mL of BPT, known to only cleave the C-terminal end VP1 sequence for this virus type[35]. We measured, 5-days post-infection, a reduction (1-$\log_{10}$) of CVA9 infectivity on BGMK cells but not on RD cells ($n = 3$, p value = 0.0116, unpaired t-test), supporting a differential infection route of the two cell lines after the C-terminal end sequence cleavage (Fig. 1f). In contrast, exposure to Subtilisin A led to a reduction of infectivity on RD cells (2-$\log_{10}$), suggesting that CVA9 is inactivated in a RGD-independent manner by this protease (Fig. 1g). This inactivation was more extensive when measured on BGMK cells (3.5-$\log_{10}$), consistent with an additional cleavage of the C-terminal end sequence by Subtilisin A ($n = 12$, p value = 0.0003, unpaired t-test with Welch's correction). While the C-terminal sequence exposed on the capsid surface of CVA9 is thus easily cleaved by both proteases, these data strongly suggest that Subtilisin A also acts on another part of the capsid of this virus type, thereby leading to virus inactivation.

Multimeric folding of capsid protomers

To further study the interaction of CVA9 with serine proteases at the molecular level, we first sought to model the smallest part of the viral capsid that accounts for the structural constraints brought by the icosahedron assembly. Our rationale led us to consider the modeling of a capsid protomer of CVA9 (heteromer: VP1, VP2, VP3) using AlphaFold2-multimer (AF2-M)[38,39]. Since the CVA9 strain used in this study was an environmental isolate, we first confirmed the amino acid conservation of all purified VPs (Fig. S3a, b) with those from the reference strain Griggs (PDB:1d4m) using mass spectrometry. Based on the sequence coverage achieved after each protein digest, we found 97.7% of VPs amino acids conservation between the environmental isolate and the reference strain (Fig. S3c–e). Due to the high sequence conservation between the environmental isolate and the reference strain, we therefore used the primary sequences of CVA9 Griggs as input for the folding process. The overlay analysis of the top one rank modeled structure on the experimental structure (PDB:1d4m) estimated an overall Root Meaning Square Deviation (RMSD) value of 2.85 Å and a model confidence of 85.2, reflecting a good quality of folding (Fig. S4a). Moreover, the representation of the protomer as a function of the predicted local Distance Difference Test (plDDT) achieved for each atom, led to identify eight viral IDPs (7 loops, C-terminal end VP1) folded with lower confidence (plDDT value < 70), which are exposed on the external surface of the capsid (Figs. 2a and S4b–f). Finally, the representation of the same protomer as a function of the Predicted Aligned Error (PAE) indicate a strong confidence of the position for each VP in the folded structure, though the position of N/C-terminal end segments (all VPs) and one loop (DE, VP1) remained imprecise (Fig. 2b). With the goal to use CVB5 and E11 as negative controls for molecular modeling experiments with serine proteases, we also modeled the two protomers of CVB5 strain Faulkner (PDB:7c9y) and E11 strain Gregory (PDB:1h8t) using the same methodology (Fig. S4g, h). The modeled structures obtained for each viral type were also predicted with high confidence (CVB5: 92.2 (rank 1), E11: 90.3 (rank 1)), though small differences in the confidence level associated with specific loops stand out between the two. For E11, the analysis also integrated a dipeptide at the C-terminal end of VP1, which was missing from the experimental structure (1h8t) and confirm the exposure of an unstructured segment (11-mer peptide) on the capsid surface.

Specific protease/virus molecular interactions

To determine the protein regions most likely involved in the interaction with serine proteases, we then used AF2-M to fold each viral protomer either with Subtilisin A or BPT. Since only Subtilisin A inactivates CVA9 in our biological experiment, we first investigated the recruitment of this protease on a CVA9 protomer. Among the top five predictive models returned by AF2-M, two showed an interaction with the DE loop of VP1, whereas two others targeted the C-terminal end VP1 sequence, all these IDPs being exposed on the surface of the capsid shell (Figs. 2c–e, h and S5a). While both CVB5 and E11 were insensitive to this protease, AF2-M nevertheless predicted an interaction between Subtilisin A and these virus types. One model returned for CVB5 (rank 1) indicated an interaction of this protease with the DE loop of VP1 (Figs. 2f, h and S5b), whereas an interaction with the C-terminal end of VP1 was predicted for E11 (rank 1 to 5) (Figs. 2g, h and S5c). We then reconducted this molecular modeling with each protomer and BPT, known to only cleave the sessile bond following an R found in tandem with the RGD motif of CVA9 C-terminal end[35] (Fig. S3c). The top five CVA9/BPT models indicated a protein contact between the protease and VP1 (Fig. 2h). However, AF2-M did not predict the interaction of BPT with the C-terminal end sequence of VP1 but instead, it suggested the recruitment of this protease on the DE loop (Fig. S5d). Comparable findings were obtained with CVB5 (Figs. 2h and S5e), while for E11 AF2-M predicted only the VP1 C-terminal end (embedding a K286) as the interacting region for BPT (Figs. 2h and S5f). The DE loop in all three virus types lacks a basic amino acid necessary for cleavage by BPT (Fig. S5g–i), yet CVA9 and CVB5 allows an interaction with this protease. We therefore wanted to rule out the possibility of a protein attachment devoid of any predictable catalytic activity. However, for all models shown above, and regardless of the serine protease used for molecular modeling, the catalytic site was found in alignment with the viral substrate surface, supporting an attempt of enzymatic attack on those viral IDPs (Fig. 2i).

Since the recruitment of serine protease to viral IDPs was not explained by enzyme specificity, we next investigated if different predicted interactions established between the protein partners might be protease/virus specific. We therefore reconducted these experiments either by truncating the C-terminal end sequence of VP1s, by substituting the full DE loops with a hydrophobic VL repeat sequence or by challenging both proteases for the same protomer during analysis (Fig. 3a–g). The presence of a hydrophobic DE loop in CVA9 (CVA9_DE loopΔVL) induced the partial or total loss of the interface between the proteases and the DE loop. However, each protease remained localized in the vicinity of this viral region during modeling, suggesting that the neighboring residues of this viral IDP also contribute to both proteases' recruitment (Fig. 3a–c). Conversely, for CVB5, we observed that replacing the DE loop with the same hydrophobic sequence favored the binding of Subtilisin A to this IDP, while reducing BPT binding to the same site (Fig. 3e). For E11, the absence of a C-terminal end on VP1 does not help Subtilisin A to consider the DE loop as an interface, unlike BPT, for which the DE loop becomes the main target (Fig. 3d). Finally, simultaneous exposure of each protomer with the two proteases revealed that BPT primarily and exclusively bound to viral DE loops, while Subtilisin A recognized the C-terminal end sequence of VP1 (Fig. 3f, g). Consequently, the protease/capsid interactions modeled by AF2-M are both virus type and serine protease specific but are not predictors for viral inactivation.

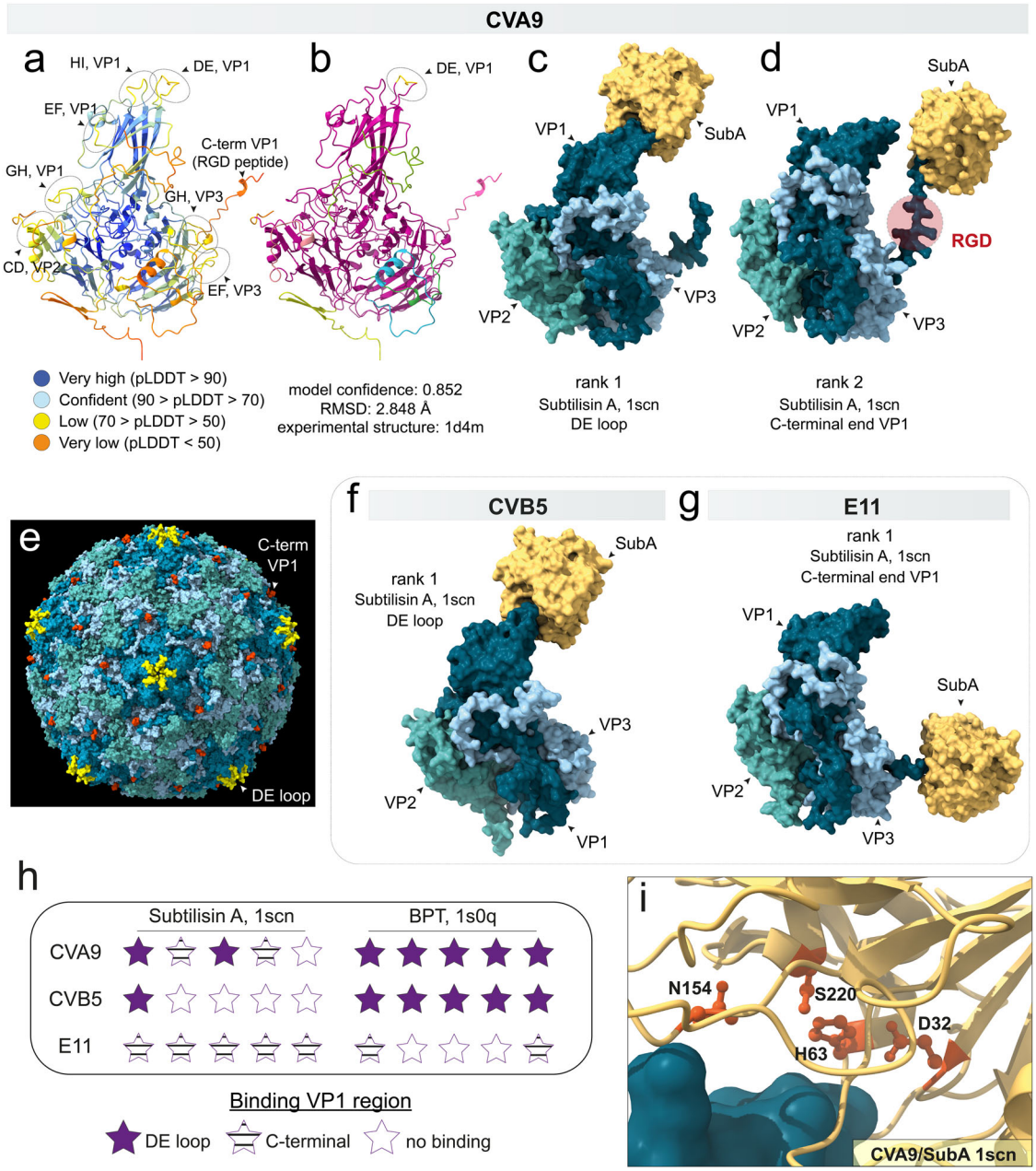

Fig. 2 | Predictive binding of serine proteases on two viral IDPs. Ribbon diagram of CVA9 protomer modeled by AF2-M (rank 1), displaying (**a**) the confidence level of the model colored by plDDT or (**b**) the confidence according to PAE score matrix. On (**a**), the circled areas correspond to jelly roll fold loops predicted with low confidence and found at least partially on the external side of the capsid shell. On (**b**), purple ribbons correspond to the residue positions well predicted by the analysis. The other colors correspond to DE loop (VP1), N-terminal VPs and C-terminal VP1, for which residue positions remain unconfirmed by the folding procedure. **c**, **d** Surface view of the two models of interaction between Subtilisin A and CVA9 protomer returned by AF2-M. **e** Surface view of CVA9 full capsid (1d4m) displaying in yellow the joining of five VP1 DE loops on the symmetry center of the 5-fold axis (vertex), and in light red the last residue resolved by X-ray diffraction, preceding the external VP1 C-terminal end segment. **f**, **g** Surface view of the models (rank 1) between Subtilisin A and (**d**) CVB5 or (**g**) E11 returned by AF2-M. **h** Overview of the predicted protein interfaces between each viral protomer and the two proteases of this study. **i** Magnified view showing the catalytic triad of Subtilisin A bordering the DE loop of CVA9 VP1. S220 corresponds to the nucleophilic serine, D32 and H63 ensure the charge relay process of the catalytic site, and N154 stabilizes the attack through the oxyanion hole formation. For all predictions, the analyses were automatically stopped after 3 simulation cycles. The experimental structures 1d4m (CVA9), 7c9y (CVB5), 1h8t (E11), 1scn (SubA, B. licheniformis) and 1s0q (BPT) have been used as template for all interface predictions.

Long-range response of protease/capsid plasticity

IDPs are characterized by high levels of plasticity and constitute attractive targets for proteases because of their inability to adopt a stable three-dimensional structure[40,41]. While our first results indicated two specific viral IDPs as target of serine proteases, we wondered to what extent the computational presence of both protein partners predicts long-range structural fluctuations for all viral IDPs. As a first investigation of the early-stage recruitment of serine proteases on viral capsid, we monitored two structural indicators (Root Meaning Square Fluctuation (RMSF) and plDDT) after the computational exposure of each viral protomer to BPT and Subtilisin A. The degree of modification of both flexibility and disorder on each VP backbone, expressed by ΔRMSF and ΔplDDT respectively (Fig. S6a, b), led to identify distinct plasticity responses depending on the viral types and the proteases considered (Figs. 4a–c and S6c–e). For VP1s, predicted to be the target of

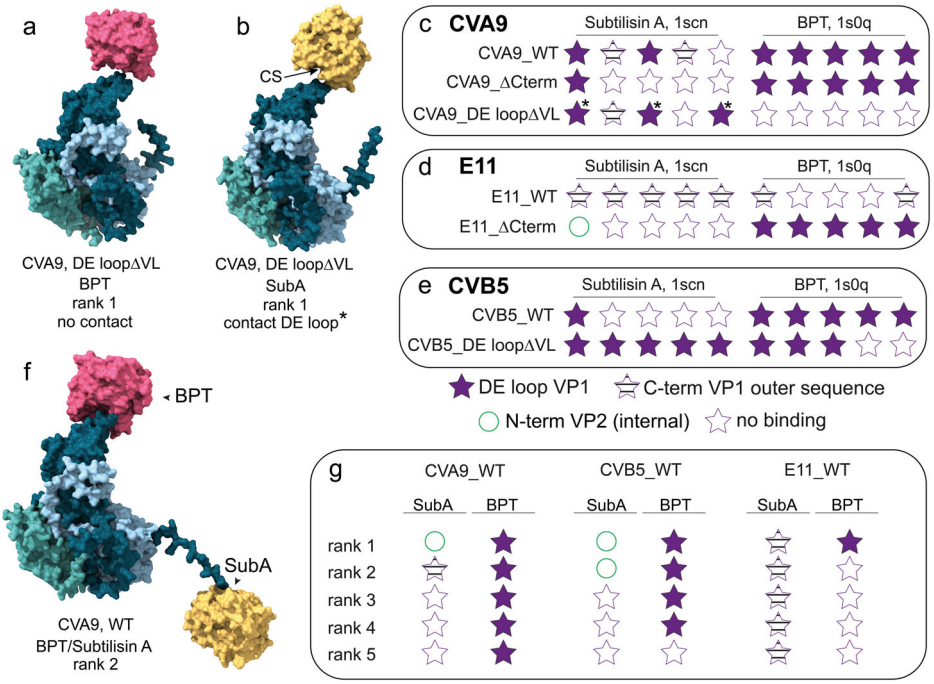

Fig. 3 | Protease/capsid interfaces are virus- and protease-specific. a Surface view of BPT recruitment on CVA9 protomer showing the loss of interface between the viral DE loop and the protease after the full substitution of the DE loop by a VL repeat sequence. **b** Surface view of Subtilisin A recruitment on CVA9 protomer a partial loss of interface between the viral DE loop and the protease after the full substitution of the DE loop by a VL repeat sequence. **c** Overview of predicted interfaces of Subtilisin A and BPT with CVA9 protomer (CVA9_WT), compared with the protomer version whose C-terminal sequence has been completely truncated (CVA9ΔCterm) or with the hydrophobic DE loop protomer mutant (CVA9_DE loopΔVL). **d** Overview of predicted interfaces of Subtilisin A and BPT with the E11 protomer (E11_WT), compared with the protomer version whose C-terminal sequence has been completely truncated (E11ΔCterm). **e** Overview of predicted interfaces of Subtilisin A and BPT with CVB5 protomer (CVB5_WT), compared with the hydrophobic DE loop protomer mutant (CVB5_DE loopΔVL). **f** Surface view of a simultaneous recruitment of BPT and Subtilisin A to both CVA9 protomer IDPs. **g** Overview of the predictive interfaces during a modeling in presence of the two serine proteases for each viral protomer. CS catalytic site, (*) used to indicate predictive outputs showing an interaction between Subtilisin A and the DE loop, for which the CS is no longer aligned with the viral sequence. All AF2-M predictions have been done with three simulation cycles.

both serine proteases, the most apparent RMSF and plDDT fluctuations were found in three loops (BC, DE, HI) and in the N-/C-terminal regions of the protein (Fig. 4a–c). However, the extent of such variation measured with both indicators appears to be greatest for CVB5 VP1 (Fig. 4b), compared to CVA9 (Fig. 4a) and E11 (Fig. 4c), also suggesting that each viral type displays a specific plasticity fingerprint during computational exposure to each protease. In addition, no association between the prediction of a contact with the DE loop or the C-terminal end VP1 and the presence of fluctuations could be made, suggestive of long-distance interactions between both protein partners. Subtilisin A and BPT are both predicted to physically interact with the DE loop of CVA9, yet they do not induce the same structural fluctuation responses (ΔRMSF, ΔplDDT) on this IDP segment (Fig. 4a). Conversely, for all E11 protomer models predicting a contact of Subtilisin A with the C-terminal end of VP1, more variable fluctuations in several loops were also found for both indicators (Fig. 4c). Lastly, the analysis of these profiles for VP2 and VP3 from each viral type, which are not involved in the prediction of protease/capsid interfaces, also led to the identification of specific plasticity fingerprints for these two proteins (Fig. S6c–e). To visualize these fluctuations on the entire capsids and thus better understand the protease/capsid structural variations, the ΔRMSF and ΔplDDT were projected onto the experimental assembly structures of each viral type (Figs. 4d and S6g). For CVA9 and CVB5 but not E11, Subtilisin A challenges the 5-fold vertex by concomitantly promoting a rigidification of the backbone and an increase in the local disorder of this region (VP1: BC, DE, HI loops) (Fig. 4d). Comparatively, BPT induces a similar response around the 5-fold center of CVB5; however, the plasticity of the same region in E11 and CVA9 is considerably less challenged under similar conditions (Fig. S6g). Finally, we applied the same methodology to study the structural fluctuations incurred by the two serine proteases when exposed to the three viral protomers (Figs. 4e, f and S6f, h, i). Similar ΔRMSF and ΔplDDT profiles were observed for each enzyme during exposure with each protomer, except for Subtilisin A during exposure with E11, which shows a less pronounced ΔplDDT profile than when exposed to CVA9 and CVB5 (Figs. 4e, f and S6f). Projecting these fluctuations onto the structures of each protease led to the identification of the region surrounding the catalytic sites of each enzyme as the most prone to structural shifts, though specific fingerprints could also be measured on each enzyme depending on the viral type exposed (Figs. 4e, f and S6h, i).

Temporal evolution of protease/protomer binding

The conformational adaptation over time of a protease on a substrate is the prerequisite for any enzymatic cleavage. Consequently, we assumed that the temporal stability of protease/protomer complexes and the spatial mobility response of viral IDPs involved in these interactions might be discriminating predictors for viral inactivation. To investigate this concept, we used AF2-M as a timelapse simulator of the molecular recruitment of Subtilisin A and BPT on CVA9, CVB5 and E11 capsid protomers. Since adding iterative cycles throughout the network ("recycles") refines the structure of multimeric models[42], we used this parameter to refine protease/virus interfaces. The number of simulation cycles during the molecular modeling was increased (6 simulation cycles) and we analyzed each recycling output as a unique time point of the prediction. During the recruitment of Subtilisin A on CVA9 protomer, only the first two ranks of the analysis predicted a contact between VP1 DE loop and this enzyme (Fig. 5a). For the first timelapse (rank 1), the number of interatomic contacts (ICs) between Subtilisin A and the CVA9 vertex indicated a significant contact area during the first four simulation cycles (IC_{max} = 54, c2), suggesting that in absence of effective cleavage, Subtilisin A continues to stably interact with this capsid region (Figs. 5a and S7a). In the second timelapse (rank 2), we also observed a contact between the DE loop and the enzyme, however the number of ICs was lower (IC_{max} = 30, c2), concomitantly leading to the recruitment of the enzyme by the C-terminal VP1 end segment and Subtilisin A unhooking from the DE loop (c5, IC = 2) (Figs. 5a and S7b, c). We previously predicted the interface of Subtilisin A with the DE loop of CVB5 (Fig. 2f) using a fast

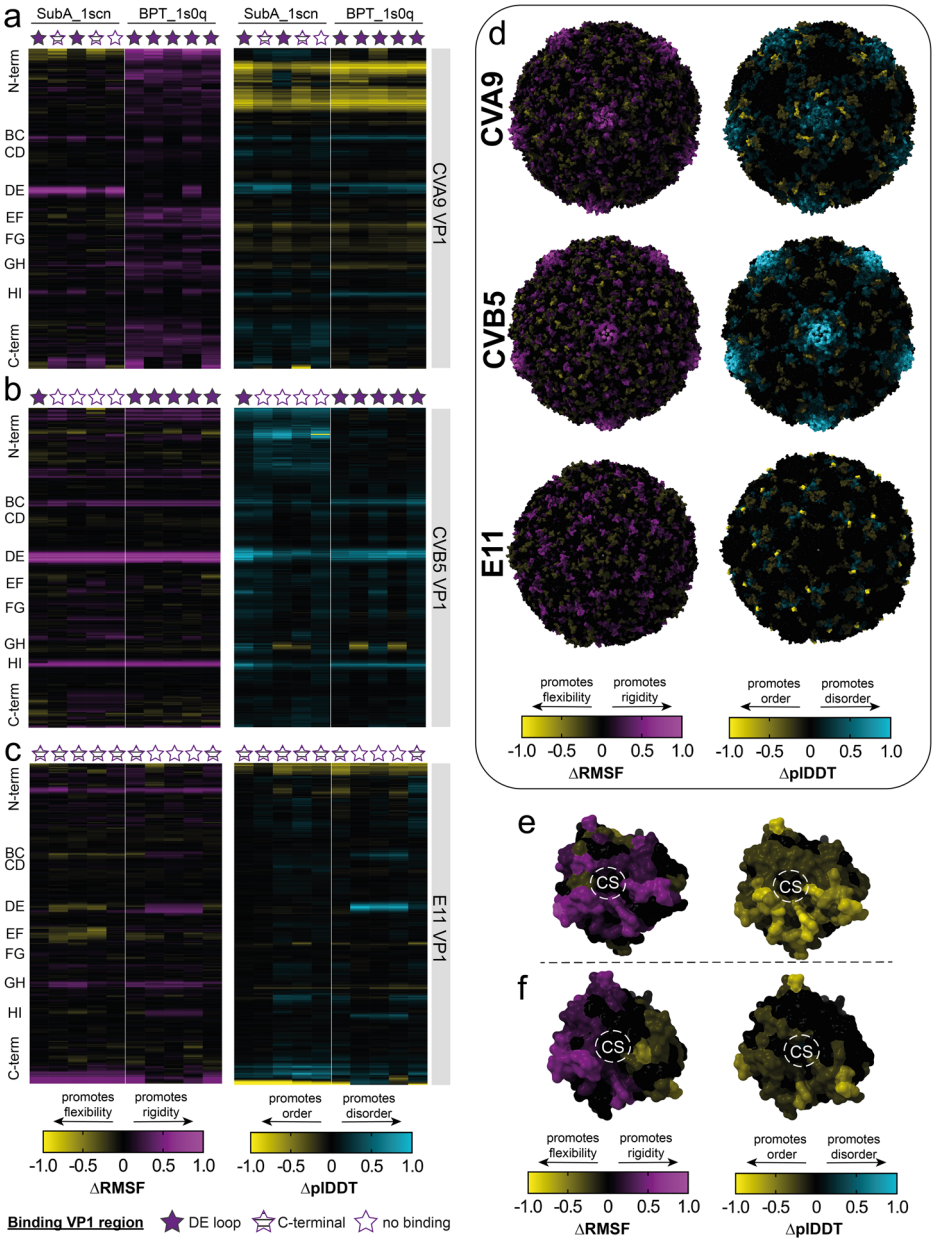

Fig. 4 | Both viral capsid IDPs and serine protease plasticity are challenged during protease/capsid exposures. Distribution of VP1 flexibility (ΔRMSF) or disorder (ΔplDDT) variations induced by Subtilisin A or BPT for (**a**) CVA9 (**b**) CVB5 and (**c**) E11. On the left of each heatmap, annotations correspond to the position of each IDPs in the viral sequence. On the top of each heatmap, stars indicate the predictive binding regions for each protease used, as mentioned above. On the top end of the first heatmap is indicated the name of the protease used in the analysis. **d** Surface view of each viral capsid colored by ΔRMSF (left part) or by ΔplDDT (right part) for each virus type after an exposure with Subtilisin A. All the capsids have been centered on the 5-fold axis view. Surface view of Subtilisin A colored by ΔRMSF (left part) or by ΔplDDT (right part), after an exposure with (**e**) CVA9 protomer or (**f**) E11 protomer. CS catalytic site. All profiles variations have been calculated based on AF2-M models folded using three simulation cycles.

automated prediction set at 3 simulation cycles, however this virus type was not inactivated in our biological assays (Fig. 1b). By increasing the computational time (6 simulation cycles) during the predictive recruitment of Subtilisin A to CVB5 protomer, we demonstrate that this protease interacts with the DE loop (rank 2), but this contact was likely too furtive (c1, IC_{max} = 13) to correlate with any biological activity (Fig. S7d). In contrast, a stable interaction with Subtilisin A was identified at the N-terminal end of VP2 for this virus type (rank 1), though this protein region is located inside the capsid and therefore not accessible in a full virus capsid. We finally confirmed that Subtilisin A does not interact with the DE loop of the 5-fold vertex of E11, but that the interaction with the C-terminal VP1 end of this viral type was maintained over time and could constitute a strong enzymatic trap for this protease (Fig. S7e).

Though BPT did not induce inactivation for any of the three viruses, we previously predicted its interaction with the DE loop of CVA9 and CVB5 (Fig. 2h). To confirm the robustness of these predictions, the 6-simulation cycles modeling protocol was applied for all three virus types with BPT and confirm the initial predictions (Fig. S7f–h). More specifically, the interaction of BPT with VP1 DE loop in CVA9 describes the prediction of 32 ICs after 4 simulation cycles, this interaction being maintained during the last three cycles of the analysis. For CVB5, we noted a greater number of ICs with the VP1 DE loop (IC_{max} = 59, c2) than for CVA9 VP1 DE loop (IC_{max} = 32, c4), suggesting that BPT binds more strongly to the vertex of CVB5, yet is not able to use this protein portion as a substrate. Finally, for E11, the molecular modeling confirmed the interaction between BPT and the C-terminal end of VP1. Therefore, all the results obtained in the presence of BPT strongly predict a trapping of the enzyme on the three viral types, which does not lead to virus inactivation. While increasing recycling strengthens predictions of potential interfaces and eliminates weaker ones, it remains however imprecise to predict virus inactivation due to the trapping of some proteases on non-functional viral IDPs.

CVA9 sensor response induced by Subtilisin A

Since increasing the number of simulation cycles strengthened the previous virus/protease interface predictions, we finally used this strategy to refine the understanding of the molecular recruitment of Subtilisin A on CVA9, which leads to virus inactivation. Besides the interaction with the DE loop, analyses conducted with 6 simulation cycles indicated the

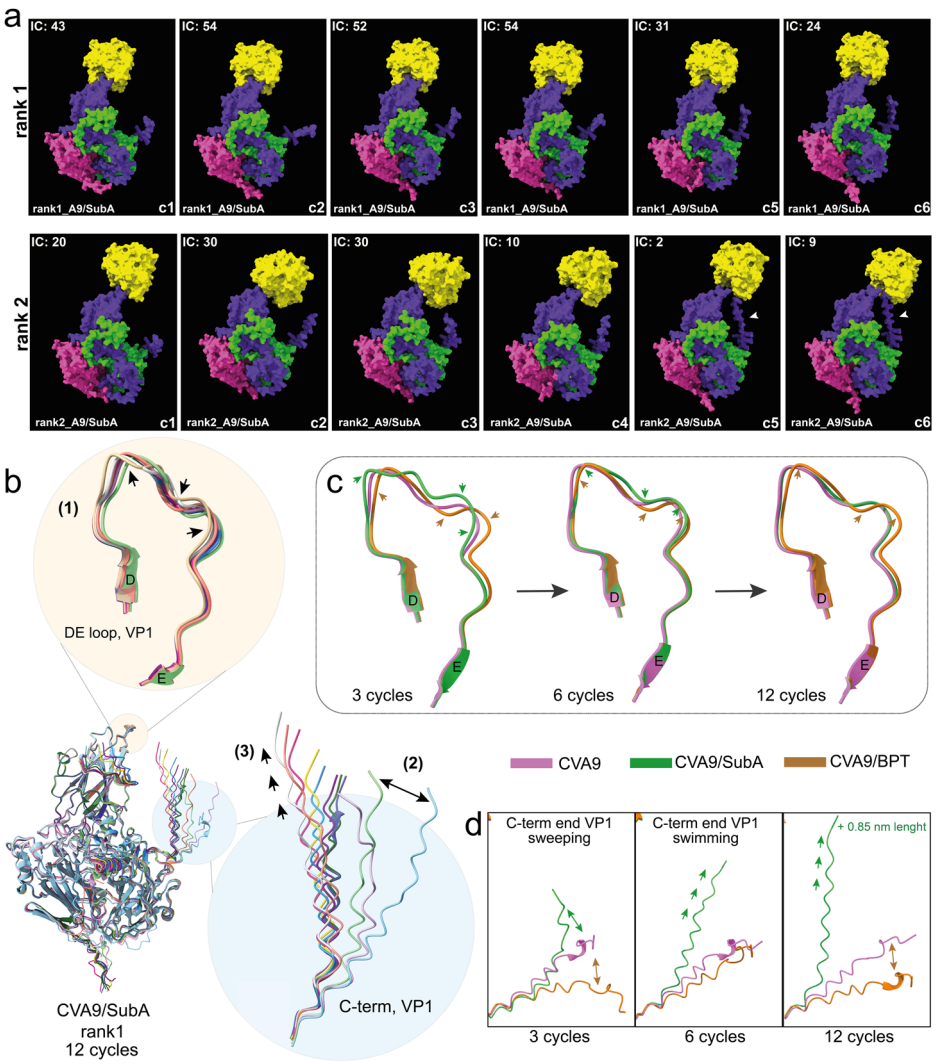

Fig. 5 | Subtilisin A induces swinging of CVA9 VP1 DE loop and leads to a fight-sensor swimming response of the C-terminal end VP1 sequence. a Predictive timeline of Subtilisin A recruitment to CVA9 protomer. For the two ranks showing a binding to Subtilisin A, each timeline is composed of 6 simulation cycles and the number of interatomic contacts (ICs) is specified in each frame. **b** Analysis of the recruitment of Subtilisin A on CVA9 capsid by overlaying the CVA9 protomer modeled during 12 simulation cycles in the presence of the enzyme. Subtilisin A was removed from the structural file to better assess predictive viral protein trajectories. On the upper part of the figure, (1) the swinging effect indicates the predictive trajectory induced by a binding with Subtilisin A to the VP1 DE loop. On the right part of the figure, (2) the sweeping effect and (3) the swimming effect correspond to the two sensor-response trajectories of the VP1 C-terminal end segment. **c** Comparative trajectories induced by Subtilisin A and BPT binding on the VP1 DE loop of CVA9 after 3, 6, and 12 simulation cycles. **d** Comparative sensor-response trajectories observed after binding of the DE loop with Subtilisin A or BPT. On the right representation, 0.85 nm corresponds to the maximum additional distance swam by the VP1 C-terminal end segment (stretched form) after 12 simulation cycles with Subtilisin A.

recruitment of Subtilisin A by the C-terminal end VP1 sequence, this phenotype not being observed with BPT. Therefore, we hypothesized that the local recruitment of the C-terminal end sequence to the DE loop binding Subtilisin A might be a defensive response to the enzymatic cleavage hazard pressure on this IDP. Molecular timelapse prediction of Subtilisin A recruitment to CVA9 protomer were thus reconducted by increasing the computational time up to 12 simulation cycles. The resulting captures indicate that the C-terminal end VP1 sequence is predicted to act both as a DE loop competitor substrate (Video S1) or as a DE loop protective peptide (Video S2), both mechanisms ultimately leading to 5-fold vertex protection. To better visualize the spatial mobility of viral protein elements during predictive enzymatic attack, the structures resulting from each cycle were overlaid (rank 1, $n_{cycles} = 12$) (Fig. 5b). While the DE loop shows a swinging motion (1) in response to a physical contact with Subtilisin A, the C-terminal end VP1 sequence, which shows a sweeping trajectory during the first cycles (2), seems to be quickly forced to adopt a swimming motion towards the 5-fold vertex (3). To illustrate that this virus response was exclusively encountered in the presence of Subtilisin A, we overlaid the structures of CVA9 modeled with or without BPT or Subtilisin A to compare the trajectories of these regions of interest over 12 cycles (Fig. 5c, d). After 3 cycles, the mobilization of the DE loop by BPT and Subtilisin A results in a strong misalignment of this viral IDP, as compared to the position taken by the loop backbone in absence of protease (Fig. 5c). After 6 cycles, a better alignment of the DE loop with both proteases was observed, compared to the condition without protease. Finally, after 12 cycles, no difference in DE loop trajectory was observed between the modeling without protease and the one with Subtilisin A, indicating that the recruitment of the enzyme by the C-terminal end sequence of VP1 allows the DE loop to recover its native position. For BPT, no visual difference was observed following 12 cycles of analysis compared to the models obtained after 6 cycles, suggesting that the presence of the BPT freezes the spatial mobility of the DE loop over time, and this regardless of the presence of cleavage site on the loop. Similarly, we analyzed the different trajectories taken by the C-terminal end VP1 sequence in presence of serine proteases in the computational environment. During the initial cycles of the analysis mimicking the contact of both Subtilisin A and BPT with the VP1 DE loop, we observed that this IDP adopted a sweeping motion, this trajectory being not observed in absence of protease (Fig. 5d). Whereas this trajectory was maintained in the presence of BPT during higher cycles, the C-terminal end sequence took a completely different path following the contact of Subtilisin A with VP1 DE loop. Indeed, after 6 cycles, the C-terminal end segment began a progressive swim towards the center of the 5-fold vertex of the virus capsid, this process resulting in an additional elongation of the C-terminal end sequence (up to 0.85 nm), sufficient to unhook the protease from the DE loop (Fig. 5d and SI Video 2). Therefore, these predictions suggest that the enzymatic pressure of Subtilisin A on the DE loop most likely acts as a sensor to drive the protective recruitment of the C-terminal end VP1 sequence to the 5-fold vertex of CVA9 capsid.

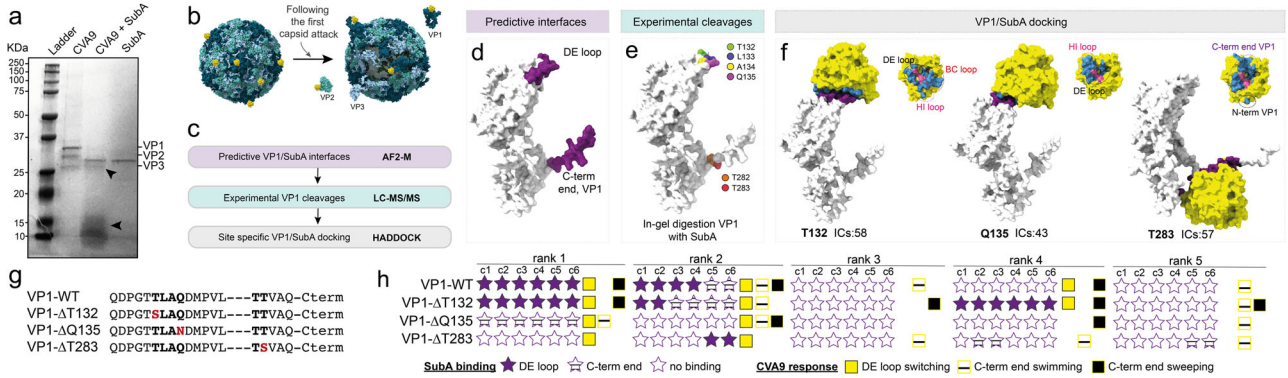

Fig. 6 | Three CVA9 VP1 amino acid residues contribute to the recruitment of Subtilisin A to CVA9 capsid and are structurally compatible to enzymatic cleavage. a SDS-PAGE analysis of CVA9 capsid protein integrity following the digestion of purified native virus in solution with Subtilisin A. The two arrows point the proteolytic viral fragments observed after 15 min digestion with Subtilisin A. **b** Schematic representation of the disintegration of CVA9 viral capsid following the predictive attack of VP1 on the 5-fold vertex and subsequent use of each independent viral protein as substrate. **c** Deductive inference process used to identify amino acid residues involved in CVA9 inactivation by Subtilisin A. **d** Surface representation of the two interfaces (in purple) predicted by AF2-M to interact with Subtilisin A during the early stages of CVA9 inactivation. **e** Mass spectrometry identification of the six amino acid residues for which the C-terminal peptide bond was cleaved following in-gel digestion of denatured VP1 with Subtilisin A. **f** Site-directed docking of Subtilisin A on three of six amino acid residues deduced during the two first steps of the selection process. Protein/peptide docking have been performed using HADDOCK 2.4 and interatomic contacts (IC) for each output have been determined using Prodigy. Surface views of Subtilisin A contact points with each VP1 regions are shown to the right of each docking structure. Pink surface regions correspond to the catalytic triad of the enzyme. **g** Point mutations of VP1 applied in silico and used to predict the significance of each amino acid residue in Subtilisin A recruitment on viral capsid. On the left of the dotted line, the sequence corresponds to the DE loop and on the right, the five first amino acid of the C-terminal end of VP1. **h** Influence of CVA9 VP1 point mutations on the prediction of Subtilisin A recruitment to viral capsid. Subtilisin A recruitments on CVA9 protomer were predicted with AF2-M using 6 simulation cycles. To the right of each prediction (rank 1 to 5), the squares represent the response of both DE loop and C-terminal end sequence trajectories. The absence of a square indicates that the corresponding trajectory event was not observed for any of the analysis.

Site-specific inactivation of CVA9 by Subtilisin A

To resolve the identification of cleavages on capsid regions leading to viral inactivation, we finally compared experimentally determined cleavage sites with predictive structural ones obtained for CVA9 following an exposure to Subtilisin A. We first treated purified CVA9 virions with Subtilisin A before analyzing all capsid degradation products by SDS-PAGE (Fig. 6a). The treatment induces a distinctive loss of the two bands corresponding to proteins VP1 (33.8 kDa) and VP2 (28.4 kDa) (CVA9 + SubA), providing evidence for the inactivation of CVA9 by capsid degradation and indicating that both VP1 and VP2 are ultimately involved in the enzymatic race dynamics of Subtilisin A (Fig. 6a, b). Findings were less conclusive for the VP3 protein, where exposure to Subtilisin A yielded a band at 26.5 kDa, very close to the expected mass of VP3 (26.3 kDa) (Fig. 6a). Since VP1 was confirmed to be cleaved by Subtilisin A treatment, we subsequently used a deductive inference process to trace the effective cleavage sites of the enzyme on this protein (Fig. 6c). We used the two interfaces predicted by AF2-M as a coarse screening of Subtilisin A cleavage sites (Fig. 6d) before confirming these predictions by protein mass spectrometry analysis. Finally, to assess enzyme/substrate accessibility during viral inactivation, each experimentally confirmed cleavage site was subjected to a site-specific molecular docking analysis with Subtilisin A using HADDOCK 2.4[43]. Of the 80 cleavage sites identified after in-gel digestion of VP1 with Subtilisin A, four were identified on the DE loop (T132, L133, A134, Q135) and two on the C-terminal end part of the protein (T282, T283) (Figs. 6e and S8a–d.). To discriminate whether cleavage of this VP in denatured form could also occur in a folded form, we used VP1 and Subtilisin A protein structures modeled by AF2-M to generate site-directed molecular docking between each residue preceding a cleavage event by Subtilisin A and the catalytic site residues (H32, D63, N154, S220) (Fig. S8e). For the six residues identified as potential targets of Subtilisin A on CVA9, three of them (T132, Q135, T283), showed a distance of less than 3 Å with the nucleophilic serine of Subtilisin A (S220), indicative of hydrogen bonding between the two partners (Figs. 6f and S8f). For each refined docking, we also analyzed the contact areas between the enzyme and the viral substrate, which indicated a number of ICs ranging from 43 to 58 depending on the sites of action (Fig. 6f). Previously, we found that the BC and HI loops may contribute to the recruitment of Subtilisin A to CVA9 (Figs. 4a and S7a). We indeed noticed that these two loops also physically interact with the enzyme during docking (Figs. 6f and S9a). Specifically, the docking targeting T132 indicates that Subtilisin A uses the HI and BC loops of VP1 to stabilize the protease/VP1 complex. For docking targeting Q135, the HI loop of VP1 also provides a support for the enzyme. Moreover, the overlay of Subtilisin A-binding VP1 on a CVA9 VP1-pentamer indicates that loops of adjacent VP1s also contribute to protease fitting on the 5-fold vertex (Fig. S9b). Finally, for the docking of Subtilisin A on the C-terminal end sequence (T283), we identified the N-terminal region of VP1 and a part of VP3 surface as additional contact area for interaction (Figs. 6f and S9c). During the attack on the three sites most likely responsible for CVA9 capsid degradation, Subtilisin A therefore fits other capsid regions before proceeding with enzymatic cleavage.

Site-specific viral response

To finally gain an understanding of the role of each residue targeted by Subtilisin A in the viral response, we generated in silico substitutions on each residue of interest before predicting the phenotypic effect of each mutation with AF2-M. To preserve the hydropathy of the viral regions as much as possible, each amino acid residue was replaced by a residue with a similar side chain and with the closest hydropathy index (H_i) of the original residue (Figs. 6g and S9d). The predictive impact of mutations T132ΔS132 and Q135ΔN135 led to the identification of two different responses in presence of Subtilisin A (Fig. 6h). Specifically, we noticed, in comparison with VP1-WT, that a substitution of T132 (VP1-ΔT132) did not cause any measurable negative effect on the ability to predict the DE loop and the C-terminal end sequence as interfaces for Subtilisin A, and similar conclusions were obtained regarding the response trajectories of both protein moieties. Conversely, we observed that the Q135ΔN135 (VP1ΔQ135) mutation led to the complete loss of prediction of the DE loop as an interface for the enzyme, thus suggesting that this residue plays a crucial role in enzyme/substrate recognition. However, this mutation does not prevent Subtilisin A from considering the C-terminal end VP1 sequence as an interface, nor does it

appear to abrogate the different types of viral mobility responses (Fig. 6h). Similar analyses were conducted with residues L133 (L133ΔI133) and A134 (A134ΔV134), which are experimentally targeted by Subtilisin A using denatured VP1 but are not structurally accessible on the native form of the protein (Fig. S9d–f). The predictive results returned for these two conditions maintain the DE loop and the C-terminal end sequence as interfaces for Subtilisin A and demonstrate similar mobility responses, thus contributing to discredit these two residues in the early stages of enzyme/substrate recognition. Finally, a similar approach was conducted on residues T282 and T283 (C-terminal end VP1), for which the peptide bond is cleaved by Subtilisin A, though only T283 indicated to be structurally compatible for cleavage (Figs. 6g and S9d). For the VP1-T283 mutant (T283ΔS283), we observed a partial loss of recognition of the DE loop as interface for Subtilisin A, compared to the VP1-WT condition. However, no change was observed regarding the recognition of the C-terminal end of VP1 by this protease (Fig. 6h). We also noticed that the mobility of the DE loop was conserved, as well as the ability of the C-terminal end sequence to adapt an extended shape (swimming trajectory). However, the mutation T283ΔS283 no longer allows the sweeping motion of the C-terminal end sequence, suggesting that this trajectory contribute very likely to the DE loop mobility during the Subtilisin A recognition process. For VP1-T282 mutant (T282ΔS282), we observed some variability in the prediction of the C-terminal end sequence as interface, but this mutation doesn't abrogate the ability of Subtilisin A to consider the DE loop as interface (Fig. S9e). Furthermore, no change in the mobility response of VP1-IDPs was observed with VP1-T282, indicating that this residue is poorly involved in DE loop swinging effect, as well as in multi-axial movements of the VP1 C-terminal end sequence. Therefore, of the two CVA9 DE loop residues targeted by Subtilisin A that most-likely lead to viral inactivation, one of them (Q135) is also crucial in the protease's recognition process on the 5-fold vertex. Furthermore, T283, found on the C-terminal end VP1 sequence, is the initiator residue of the sweeping motion, thereby acting as a sensor residue to facilitate enzyme recognition on the DE loop.

Discussion

While the repertoire of extracellular bacterial serine proteases found in aqueous environments contributes to the extra-host inactivation of enteroviruses[3], the underlying molecular mechanisms explaining such an outcome remained unexplored. Accordingly, we provided here a first overview of the structure/function relationship between these enzymes and miniatures versions of enterovirus capsids (protomer; capsid portion: 1/60th), thereby leading to a better understanding of protease-mediated inactivation.

For the three virus types used in this work (CVA9, CVB5, E11), only CVA9 was sensitive to both serine proteases studied (Subtilisin A, BPT), corroborating previous data which suggest an atypical sensitivity of this virus type to proteolytic enzymes[4]. Furthermore, we demonstrated that both proteases cleave the C-terminal end sequence of CVA9 without altering virus infectivity[35,36], but only Subtilisin A inactivate CVA9 in a host-independent manner. These experimental findings can be rationalized by an integrative computational approach, combining the prediction of protease/capsid interfaces and a site-specific docking refinement. Consequently, the absence of a stable interface between Subtilisin A and the DE loops of the 5-fold vertex of CVB5 and E11 explains the proteolytic resistance of both viruses. Conversely, CVA9 DE loops predict an interface with Subtilisin A, and the molecular docking refinement targeting two loop residues explains CVA9 sensitivity to inactivation in a host-independent manner. Predictions of interfaces with BPT for all viruses indicate that DE loops interact with this enzyme, yet the three viruses are insensitive to proteolysis in a host-independent manner due to the absence of a specific cleavage site (K, R). Finally, site-directed docking analyses of CVA9 C-terminal end residues (T283: Subtilisin A; R288: BPT) explain the cleavage by both proteases, leading to the loss of the RGD motif used for integrin recognition in BGMK cells.

While BPT cleaves a limited number of substrates (R, K), Subtilisin A is expected to cleave a broad range of substrates[29]. Accordingly, the analysis of Subtilisin A cleavage sites by mass spectrometry identified 199 cleavage sites on all CVA9 denatured VPs, while a similar experiment with BPT identified 46 sites on the same viral substrate. However, viral inactivation experiments using cell culture confirmed that Subtilisin A's specificity is not the sole parameter explaining *Enterovirus*'s capsid disintegration. Though CVA9 is easily inactivated with Subtilisin A, E11 and CVB5 are resistant to this protease, supporting the crucial role of structural protease/capsid compatibility to explain virus inactivation. Finally, the SDS-PAGE analysis of CVA9 capsid products following an exposure to Subtilisin A confirmed the degradation of all capsid VP1s and VP2s, and probably some VP3s, indicative of capsid disintegration for this virus type.

While viral inactivation mimicked the reactional endpoint of enzyme catalysis, the intermediate steps leading to such a phenotype remained to be demonstrated. Thanks to the release of AF2-M[38], we reconstructed with accuracy enterovirus capsid protomers, subsequently facilitating the functional study of protease/capsid complexes by molecular modeling. By selecting CVA9 as a serine protease sensitive virus and CVB5 and E11 as insensitive viruses to challenge our hypotheses, we sequentially reassembled the molecular steps leading to enzymatic cleavage of viral capsids. As such, we propose a three-step predictive molecular mechanism to explain the recruitment of these enzymes on such giant substrates:

(1) Precognition: before any physical contact between serine proteases and viruses, the co-presence of both partners in the same environment led to structural fluctuations highly predictive of long-range electrostatic interactions[44]. These interactions have already been described as a modulator of folding stability of IDPs[45,46], and contribute to the determinism and stability of serine proteases for substrates[47,48] as well as to the functional modulation of some allosteric enzymes[49,50]. For each modeling performed with serine proteases and viral protomers, we mainly observed those fluctuations on viral IDPs and on regions surrounding the active sites of each protease, which is highly consistent with the findings cited above. Moreover, we point out different flexibility responses depending on the partners used, also suggesting that long-range interactions are both protease and viral substrate specific. Therefore, we suggest the contribution of long-range electrostatic interactions as an early stage of enzyme-substrate communication, which modulate both viral capsid and protease plasticity.

(2) Recognition: as a second step of interaction, we described the physical contact of serine proteases to some accessible IDPs segments of viral capsids (VP1: DE loop, C-terminal end). Due to the inability of IDPs to adopt a well define structural conformation, those sequences are known to depict disorder-to-order transitions states upon binding[51], making them also sensitive to proteolysis[52]. Though viral IDPs have not been described as potential target of serine proteases, two studies indicate that both subtilisins and trypsins may favor the cleavage of accessible disorder segments in other native proteins[41,53]. However, we noticed that AF2-M prediction of protease binding to viral IDPs was not a binary indicator of enzymatic cleavage, but more an essential first contact to initiate a functional or a non-functional enzyme-substrate binding. Indeed, two facts pointing in this direction have emerged from this work, including the long-term binding of BPT to both CVA9 and CVB5 VP1 DE loops containing no effective cleavage site, and the brief binding of Subtilisin A to the DE loop of the CVB5 capsid, neither of which resulted in protein cleavage. While increasing the number of recycles during modeling can be valuable to refine structure prediction[54], the modulation of this parameter also brings robustness to temporality and strength of protease/capsid interfaces. As a result, the interface of Subtilisin A with CVB5 DE loop was abrogated, but the non-functional binding of BPT with the DE loop of capsids was maintained. We therefore propose that this recognition step does not depend on the specificity of action of serine proteases for viral substrates, but rather on the strength of short-range interactions (i.e. van der Waals forces, hydrogen bonding) between the two protein partners, which further accommodates the "fight or flight" response of serine proteases on viral capsids.

(3) Adaptation: finally, the last step of enzyme/substrate communication achieved by site-specific molecular docking refinement mimics a protease/capsid structural adaptation, which is decisive for initiating any enzymatic cleavage. Though the active site of Subtilisin A physically binds the two CVA9 VP1 IDPs segments cleaved by the protease (DE loop, C-terminal end), the enzyme also adapts locally to other regions of the viral capsid to initiate catalysis. Indeed, the C-terminal end portion of CVA9 VP1, which seems to act as a "crazy horse" with a great ability to elongate and move in space, fits locally on either side of the active site on the 5/2 axis of the capsid shell during molecular docking refinement. Similarly, the DE loop targeted by Subtilisin A, adapts its positioning on either side of the catalytic center with the adjacent BC and HI loops, these loops being described to contribute greatly to the plasticity of the 5-fold vertex of enteroviruses capsids[10,55]. Accordingly, we suggest that the adaptation step, which corresponds to the discriminative phase of protease-capsid interaction, clearly approximates the induced-fit model proposed by D. Koshland[56].

While the presence of single mutations in a protein sequence is described to have minimal impact on the folding predicted by AlphaFold and on the overall stability of proteins[57], our results indicate however that such mutations can modulate both protease/capsid interfaces prediction. For all single mutations generated in silico on the three effective cleavage sites of Subtilisin A on CVA9 VP1, AF2-M predicted a partial or complete loss of contact of the enzyme with the capsid VP1 DE loop depending on the viral mutant. Moreover, we also observed spatial mobility alterations of the C-terminal end VP1 sequence, thus suggesting that the effective residues of the viral substrate are involved in both the early recruitment of the enzyme on the capsid and the VP1 structural mobility response. Consequently, though the general recognition process of serine proteases on enterovirus capsids seems broadly similar, we point out that the side-chain chemistry of the targeted residues during catalysis, and by extension the predictable intermolecular forces engaged by these residues in the interaction with Subtilisin A, contribute to the specific interaction protease/capsid leading to viral inactivation.

Overall, we provide a first methodological framework to investigate the functional characterization of serine proteases involved in the race for the disintegration of non-enveloped viruses in aqueous environments. Due to the high number of enzymatic reactions described to date and their roles in systems biology (*e.g.* microbial control, cancer research, food preservation), this advance will more generally speed up the knowledge on molecular mechanisms of protease/substrate interactions.

Methods

Cells and viruses

Buffalo Green Monkey Kidney (BGMK, provided by Spiez Laboratory, Switzerland) cells were maintained in minimum essential media (MEM, Gibco, ThermoFisher Scientific) supplemented with 10% Fetal Bovine Serum (FBS, Gibco) and 1% Penicillin/Streptomycin (P/S, Gibco). The human Rhabdomyosarcoma muscle cell line (RD, ATCC CCL-136) was maintained in Dulbecco's Modified Eagles Medium (DMEM, Gibco) containing 10% FBS and 1% P/S. Both cell lines were maintained at 37 °C (5% CO_2). The environmental isolate coxsackievirus A9 (CVA9), originating from sewage, was provided by the Finnish National Institute for Health and Welfare. Echovirus 11 (E11) and coxsackievirus B5 (CVB5) were purchased from ATCC and correspond to the Gregory strain (VR-737) and the Faulkner strain (VR-185), respectively.

Virus stocks preparation and enumeration

Each virus type was propagated by infecting sub-confluent monolayers of BGMK cells as previously described[58]. Briefly, viruses were released from infected cells following three freezing-thawing steps. Cell debris were removed by centrifugation (3000 × *g*, 5 min). After filtration of the supernatant containing viruses on a 0.2 µm syringe filter (Filtropur S, PES, Sarstedt), virus stocks were concentrated on a 100 kDa cellulose membrane (Amicon Ultra-15, Merck Millipore) and rinsed three times successively with PBS. Infectious virus concentrations were enumerated by a most probable number (MPN) infectivity assay. Virus sample aliquots (100 µL) were diluted by 10^{-1} to 10^{-8} in MEM 2% FBS. Each dilution (100 µL, 5 replicates) was plated on a BGMK sub-confluent monolayer in a 96-well plate and was incubated at 37 °C (5% CO_2). After 4 days, the number of wells with cytopathic effects (CPEs) for each dilution was recorded, and the resulting number of infectious viruses per sample was calculated using R[59]. The limit of detection (LoD) of the assay, defined as the concentration corresponding to one positive cytopathic effect in the lowest dilution of the MPN assay under the experimental conditions used, corresponds to 2 MPN/mL. Each virus stock was stored at −20 °C until use.

Protease-mediated viral infectivity reduction assay

To assess the sensitivity of enteroviruses to serine proteases, we selected two commercially available proteases (Subtilisin A from *B. licheniformis* (P5380, Sigma-Aldrich), Bovine Pancreatic Trypsin (BPT) (T1426, Sigma-Aldrich)), based on published data as explained in supplementary information[3,35]. To screen the sensitivity of CVB5, CVA9 and E11 to serine proteases, 100 µL of each virus stock (1.10^6 MPN/mL) were incubated with a final concentration of 20 µg/mL of Subtilisin A or BPT for 2 or 6 h at 37 °C. All enzymatic reactions were immediately stopped by adding 900 µL of MEM 2% FBS. Negative controls of inactivation for each virus type were performed by replacing serine proteases by PBS, following the same procedure as described above. Viral reduction infectivity was determined as $\log_{10}(C/C_0)$, where C is the residual titer after adding protease for each time point, and C_0, the titer measured without addition of protease for each corresponding time point. The experimental LoD of the assay was approximately 5-$\log_{10}$.

Flow cytometry analysis

Flow cytometry was used to determined αVβ3 and αVβ6 integrins surface expression in BGMK and RD cells. After a wash with PBS, cells were detached using trypsin-EDTA (0.05%) (Gibco) and pelleted by centrifugation (400 × *g*, 2 min) in a 96-well U-bottom plate (10^5 cells/well). Cells were washed twice in PBS and stained with 1 µg/mL DAPI (D9542, Sigma-Aldrich) for 15 min at room temperature (RT) in the dark. After two successive washes with a staining buffer (PBS, 1% bovine serum albumin), cells were incubated with a Fc receptor blocking solution (564219, BD Pharmingen) for 15 min at RT in the dark. Subsequently, cells were stained with Alexa Fluor® 488-conjugated anti-αVβ3 antibody (Novus Biologicals, USA, FAB3050G) (39.5 µg/mL) and Alexa Fluor® 700-conjugated anti-αVβ6 antibody (Novus Biologicals, NBP2-50448AF700) (30.5 µg/mL), or with isotype controls (Alexa Fluor® 488-conjugated mouse IgG1 (R&D systems, USA, FAB110G) and Alexa Fluor® 700-conjugated rat IgG2 (Novus Biologicals, IC006N) for 20 min at 4 °C in the dark. Stained cells were finally washed twice with PBS and resuspended with 200 µL PBS prior to an immediate acquisition. Data acquisitions were performed on a Gallios flow cytometer (Beckman Coulter, CA, USA), with a minimum of 5000 cells acquired per sample. Acquired data were analyzed in FloJo software version 10.8.0. Cell doublets were excluded by single cell gating, and single cells were then gated based on viability ($DAPI^-$) prior to the analysis of cell surface integrin expression ($\alpha V\beta3^+/\alpha V\beta6^+$).

CVA9 C-terminal end VP1 cleavage assessment by cell culture

BGMK and RD cells were used to monitor the cleavage of CVA9 C-terminal end segment carrying a RGD motif. First, to investigate the permissiveness of both cell lines for CVA9, roughly 10^5 MPN/mL of viruses were used to infect simultaneously 96-well plates of sub-confluent RD and BGMK monolayers following the general procedure as described above. The CPEs were monitored 3, 4 and 5 days post-infection and virus titers were calculated as mentioned above. To assess the cleavage of the C-terminal end VP1 sequence by Subtilisin A, two tubes each filled with 100 µL of CVA9 stock (1.10^6 MPN/mL) were incubated with 2 µL of Subtilisin A at 1 mg/mL for 2 h at 37 °C. After incubation, all tubes were immediately filled with 900 µL of MEM 2% FBS to stop the enzymatic reaction. The same incubation was similarly conducted with BPT

and negative controls of inactivation were performed by replacing serine proteases by PBS. All conditions were simultaneously plated either on RD or BGMK sub-confluent monolayers as mentioned above. CPEs were monitored 5-days post-infection and viral decays were calculated as described above. The experimental LoD of the assay was approximately 5-$\log_{10}$.

Virus purification

Three T-150 cell culture flasks (25 mL/flask) of CVA9-infected BGMK cells were recovered and subjected to three successive freeze/thaw cycles. The cultures were centrifuged at 3000 × *g* for 8 min and the resulting supernatants were filtered through 0.22 µm membrane. A volume of 30 mL of supernatant was dispensed in two 38.5 mL ultracentrifuge tubes (Ultra-Clear, 25 × 89 mm, 344058, Beckman Coulter) before adding 5 mL of a 20% sucrose solution in NTE buffer (100 mM NaCl, 10 mM Tris-HCl pH7.5, 1 mM EDTA pH8,) to the bottom of each tube. Each tube was centrifuged for 3 h at 150,000 × *g* (4 °C) using an Optima XPN-80 ultracentrifuge (Beckman Coulter) equipped with a SW 32 Ti swinging bucket (369650, Beckman Coulter). Supernatants were discarded by inverting tubes, and 80 µL of PBS was added to each individual pellet. After resuspension of pellets, the two samples were mixed, and the total volume of viral suspension was adjusted to 1 mL with PBS. After packing a seven-phases discontinuous sucrose gradient (15%, 20%, 25%, 30%, 35%, 40%, 50%) in a 17 mL ultracentrifuge tube (Ultra-Clear, 16 × 102 mm, 344061, Beckman Coulter), and leaving overnight to allow for merging of the layers into a continuous gradient, 500 µL of CVA9 suspension were applied on top of the first layer. The tube was centrifuged for 3 h at 150,000 × *g* (4 °C) using a SW 32.1 Ti swinging bucket (369651, Beckman Coulter). Finally, successive 500 µL fractions were collected from the bottom of the tube and stored at −20 °C until use.

SDS-PAGE analyses

SDS-PAGE was used to monitor both CVA9 purity following the two-step sucrose purification procedure and to evaluate the proteolytic degradation of viral proteins (VPs) by Subtilisin A. Prior to each SDS-PAGE analysis, 20 µL of protein sample were denatured in Laemmli buffer for 10 min at 95 °C. The protein profiles in each sucrose fraction and the identification of the purified CVA9 fraction have been analyzed on Any KD Mini-Protean TGX Precast gel (4569033, Biorad). Sample preparation of CVA9 VPs for in-gel digestion prior to mass spectrometry analyses and the assessment of the VPs degradation following Subtilisin A treatment on native CVA9 virions have been done using 12% Mini-Protean TGX precast gel (4568043, Biorad). Prior to SDS-PAGE analysis of VPs degradation products by Subtilisin A, 20 µL of the purified native CVA9 fraction were incubated either with 2 µL of Subtilisin A at 100 µg/mL or with 2 µL of PBS for 15 min at RT. For all analyses, the Dual Color standards (Biorad) has been used as protein ladder and gels were stained with Instant Blue Coomassie solution (Abcam).

In-gel digestions

Gel pieces containing the concentrated individual VPs were excised and washed twice with 50% ethanol in 50 mM ammonium bicarbonate (AB, Sigma-Aldrich) for 20 min and dried by vacuum centrifugation. Proteins were reduced with 10 mM dithioerythritol (Merck-Millipore) for 1 h at 56 °C followed by a washing-drying step as described above. Reduced proteins were alkylated with 55 mM Iodoacetamide (Sigma-Aldrich) for 45 min at 37 °C in the dark followed by the same washing-drying step described above. VPs were then digested either (1) overnight at 37 °C using mass spectrometry grade Trypsin (Pierce), GluC (Pierce) or Chymotrypsin (Promega) at a concentration of 12.5 ng/µl in 50 mM AB, or (2) for 1 h at 37 °C using Subtilisin A (P5380, Sigma-Aldrich) with the same concentration as for the three other enzymes. For Trypsin digestions, 10 mM CaCl2 was added. Resulting peptides were extracted in 70% ethanol, 5% formic acid (FA, Merck-Millipore) twice for 20 min, dried by vacuum centrifugation and finally desalted on C18 StageTips[60].

Mass spectrometry analyses

Digested-VPs were resuspended in 2% acetonitrile (ACN, Biosolve), 0.1% FA for LC-MS/MS injections. Nano-flow separations were performed on a Dionex Ultimate 3000 RSLC nano UPLC system (Thermo Fischer Scientific) online connected with an Orbitrap Lumos Fusion Mass-Spectrometer (Thermo Fischer Scientific). A capillary precolumn (Acclaim Pepmap C18, 3 µm-100Å, 2 cm × 75 µm ID) was used for sample trapping and cleaning. Analytical separations were conducted on a 50 cm long in-house packed capillary column (75 µm ID, ReproSil-Pur C18-AQ 1.9 µm silica beads, Dr. Maisch). The analysis was performed with a 250 nL/min flow rate (A: 98% H_2O, 2% ACN, 0.1% FA; B: 90% ACN, 2% H_2O, 0.1% FA) using a 90 min biphasic gradient as follow: after sample loading at 1% B, the gradient was raised to 24% B in 46 min, followed by an increase to 38% B in 10 min. After 3 min at 90% B, a final conditioning was set at 1% B for 15 min. Acquisitions were performed through Top Speed Data-Dependent acquisition mode using a cycle time of 1 s. First MS scans were acquired over a mass range of 375–1500 *m*/*z* with a resolution of 240,000 (at 200 *m*/*z*) and a maximum injection time of 50 milliseconds was used. The most intense parent ions were selected and fragmented by High energy Collision Dissociation (HCD) with a Normalized Collision Energy (NCE) of 30% using an isolation window of 0.7 *m*/*z*. Fragmented ions were acquired using the Ion Trap with a maximum injection time of 60 milliseconds. Selected ions were then excluded for the following 20 s. Raw data were processed using SEQUEST and MS Amanda[61] in Proteome Discoverer v.2.2 against the Uniprot Chlorocebus aethiops entries supplemented with VP1, VP2 and VP3 ones (from PDB 1d4m). Enzyme specificity was set either to Trypsin, GluC or Chymotrypsin and a minimum of six amino acids was required for peptide identification. Up to two missed cleavages were allowed and a 1% FDR cut-off was applied both at peptide and protein identification levels. Data were further processed and inspected in Scaffold 5 (Proteome Software, Portland, USA).

Multimeric protein folding

Both viral protomers folding and protease/virus interfaces were predicted with AlphaFold2-Multimer v2 (AF2-M)[38] using ColabFold v1.5.2[54]. Multiple sequence alignments (MSA) were generated with MMseqs2[62] against the Uniclust30 database[63], the MGnify database[64] and the PBD70 database[65] using the unpaired_paired mode. For each protein sequence inputs used for analysis, PDB templates were added to prediction: CVA9 (1d4m), E11 (1h8t), CVB5 (7c9y), Subtilisin A (1scn), BPT (1s0q). The folding of each viral protomer and the fast prediction of protease/capsid interfaces were initially performed in automatic mode using 3 recycles. To challenge the strength of protease/capsid interfaces and study the long-term binding of proteins partners, the number of iterative cycles has been increased up to 6 or 12 depending on the experiment with an early step tolerance set at 0. Topologies qualities of the folded proteins and interfaces were estimated using Template-Modeling (TM) score, interface-TM score, predicted local Distance Difference Test (plDDT) and Predicted Alignment Error (PAE) plot. The model confidence of each folded monomer or multimer was calculated as previously described[38,39]. A comparison of the overall RMSD between predictive viral protomers and the corresponding PDB structure was also used for the analysis. For the timelapse simulator experiment of protomer/protease interfaces ($n_{cycles} = 6$), the PRODIGY webserver[66] was used to assess the number of Interatomic Contacts (ICs) between each protein partner for each cycle.

Plasticity response assessment

To assess the local plasticity response of both viral protomers and proteases during the folding process, pLDDT and Root Meaning Square Fluctuation (RMSF) values were used as structural motion indicators. Both indicators were studied on all predictive protease/protomer models and compared with a predictive protease model alone or a predictive protomer alone depending on the interaction model. As such, disorder assessment was expressed as $\Delta plDDT = plDDT_0 - plDDT_1$, whereby $plDDT_0$ corresponds to the global order/disorder state of either a predicted protease or a predicted

protomer without encountering the other protein partner and $plDDT_1$ defined the plDDT output of the co-presence of both protomer and protease in the computational environment. To assess flexibility variations, the CABS-flex 2.0 standalone webserver[67] was run with the same PDB files returned by AF2-M as used above. Flexibility variations were calculated as $\Delta RMSF = RMSF_0 - RMSF_1$, whereby $RMSF_0$ corresponds to the global flexibility/rigidity state of each protein partner alone and $RMSF_1$ corresponds to the same profile during the computational exposure of both protein partners. All Δvalues, initially ranging from −40 to 40 for ΔplDDT and −8 to 8 Å for ΔRMSF depending on protomer/protease models, have been normalized between −1 to 1, whereby 0 indicate no detectable plasticity change during the folding process.

Predictive viral mutants

To assess interface competition between each protease with the DE loop and the C-terminal end of VP1 during the folding with E11 and CVA9, the VP1 sequence of each viral type was modified either by truncation or substitution. Truncated versions of VP1 were obtained by removing the C-terminal end sequence exposed at the capsid surface of E11 (11-mer: PDTVKPDVSNH) and CVA9 (18-mer: TTVAQSRRRGDMSTLNTH). To abrogate the interfaces of Subtilisin A and BPT with CVA9 and CVB5 DE loops, the 14 amino acids of each loop (CVA9: QDPGTTLAQDMPVL, CVB5: EQSTIQGQDSPVL) were substituted by seven successive repeats of LV (LVLVLVLVLVLVLV). Targeted single substitution were further done on both DE loop and C-terminal end of CVA9 VP1, following a mass spectrometry identification of effective Subtilisin A cleavage sites on those two regions. Substitutions were chosen based on hydropathy property (H_i) conservation, using the Kyte and Doolittle's index[68]. As such, all T (T132, T282, T283) were individually substituted with a S ($H_{i\ T} = -0.7$, $H_{i\ S} = -0.8$), Q135 with a N ($H_{i\ Q} = H_{i\ N} = -3.5$), L133 with a I ($H_{i\ L} = 3.8$, $H_{i\ I} = 4.5$) and A134 with a V ($H_{i\ A} = 1.8$, $H_{i\ V} = 4.2$). The effect of each modification on protease/virus interaction was assessed using AF2-M using the methodology described above.

Docking refinement

The webserver HADDOCK 2.4[43] was used to refine the interaction of Subtilisin A with each residue involved in an effective cleavage either in the DE loop (T132, L133, A134, Q135) or the C-terminal end VP1 sequence (T282, T283). For each analysis, both CVA9 protomer and Subtilisin A structures predicted with AF2-M were used as input. The VP1 was defined as protein chain A, and each targeted residues cited above was individually selected as active residue during the docking process. For Subtilisin A, defined as chain B, the four residues involved in the catalytic reaction (H32, D63, N154, S220) were selected as active residues. To assess the best conditions of analysis, we ran two different pipelines either adjusted to study protein/protein docking or peptide/protein docking. In the first experiment, all default settings were used for the analysis. In the peptide/protein docking, analysis parameters were adapted as follows: the number of structures for semi-flexible refinement, for final refinement and the number of structures to be analyzed were fixed at 400. The number of MD steps during it1 was set at 1000 steps on the high-temperature rigid body and during the first cooling stage of the rigid body, while this number during the second and third cooling stages was set at 3000. For both pipelines, and regarding the viral residue targeted for the docking, DE loop and C-terminal end sequence flexibility were considered either automated, semi-flexible or fully flexible during the analysis. For all outputs, the Fraction of Common Contacts (FCC)[69] method was used to filter the five best clusters returned by the analysis. As second filtering step, a distance analysis between the nucleophilic serine of Subtilisin A (S220) and each targeted viral residues was measured and a 3Å cut-off was applied as strong hydrogen bond indicator. Finally, the PRODIGY webserver was used to assess the overall portion of ICs.

Proteins visuals, structure editing

All protein structure visuals, which include capsid viral proteins (protomers and viral assemblies), as well as enzyme monomers and enzyme/virus interactions, and inter-residue distance measurements were performed using ChimeraX (version 1.5)[70]. All visuals were then accommodated for publication using Adobe Illustrator (version 25.1).

Statistics and reproducibility

Data normality assessment and statistical analyses used to compare both viral infectivity and surface expression of integrins were performed with GraphPad Prism v.9.5.0. Samples comparison was done by one-tailed or two-tailed *t*-test depending on sample distribution, as precised in the caption of each corresponding figures. For the analyses showing a significant difference between samples variance ($p < 0.05$), a Welch's correction was applied to each test. For all tests, an alpha value of 0.05 was used as a threshold for statistical significance.

Data availability

All Supplementary Figs. (S1–S9), including the gating strategy used for flow cytometry (S10) and all unedited protein gels (S11), are available in Supplementary Information. SI videos, modeling and docking outputs, Supplementary Data 1 and mass spectrometry data are publicly available on Zenodo[71].

Received: 10 November 2023; Accepted: 24 July 2024;
Published online: 09 August 2024

References

1. Gall, A. M., Mariñas, B. J., Lu, Y. & Shisler, J. L. Waterborne viruses: a barrier to safe drinking water. *PLoS Pathog.* **11**, e1004867 (2015).
2. Rodríguez-Lázaro, D. et al. Virus hazards from food, water and other contaminated environments. *FEMS Microbiol. Rev.* **36**, 786–814 (2012).
3. Corre, M.-H., Bachmann, V. & Kohn, T. Bacterial matrix metalloproteases and serine proteases contribute to the extra-host inactivation of enteroviruses in lake water. *ISME J.* **16**, 1970–1979 (2022).
4. Cliver, D. & Herrmann, J. Proteolytic and microbial inactivation of enteroviruses. *Water Res.* **6**, 797–805 (1972).
5. Hogle, J. M., Chow, M. & Filman, D. J. Three-dimensional structure of poliovirus at 2.9 Å resolution. *Science* **229**, 1358–1365 (1985).
6. Rossmann, M. G. et al. Structure of a human common cold virus and functional relationship to other picornaviruses. *Nature* **317**, 145–153 (1985).
7. Baggen, J., Thibaut, H. J., Strating, J. R. P. M. & van Kuppeveld, F. J. M. The life cycle of non-polio enteroviruses and how to target it. *Nat. Rev. Microbiol.* **16**, 368–381 (2018).
8. Baker, T. S., Olson, N. H. & Fuller, S. D. Adding the third dimension to virus life cycles: three-dimensional reconstruction of icosahedral viruses from cryo-electron micrographs. *Microbiol. Mol. Biol. R.* **63**, 862–922 (1999).
9. Rossmann, M. G. & Johnson, J. E. Icosahedral RNA virus structure. *Annu. Rev. Biochem*. **58**, 533–573 (1989).
10. Füzik, T., Moravcová, J., Kalynych, S. & Plevka, P. Structure of human enterovirus 70 and its inhibition by capsid-binding compounds. *J. Virol.* **96**, e00604–e00622 (2022).
11. Huang, K.-Y. A. et al. Structural and functional analysis of protective antibodies targeting the threefold plateau of enterovirus 71. *Nat. Commun.* **11**, 5253 (2020).
12. Oberste, M. S., Maher, K., Kilpatrick, D. R. & Pallansch, M. A. Molecular evolution of the human enteroviruses: correlation of serotype with VP1 sequence and application to picornavirus classification. *J. Virol.* **73**, 1941–1948 (1999).

13. Hendry, E. et al. The crystal structure of coxsackievirus A9: new insights into the uncoating mechanisms of enteroviruses. *Structure* **7**, 1527–1538 (1999).
14. Polgár, L. Chapter 3 Structure and function of serine proteases. *N. Compr. Biochem.* **16**, 159–200 (1987).
15. Wright, C. S., Alden, R. A. & Kraut, J. Structure of subtilisin BPN′ at 2.5 Å resolution. *Nature* **221**, 235–242 (1969).
16. Drenth, J., Hol, W. G. J., Jansonius, J. N. & Koekoek, R. A comparison of the three-dimensional structures of subtilisin BPN' and subtilisin novo. *Cold Spring Harb. Sym. Quant. Biol.* **36**, 107–116 (1972).
17. Bode, W. & Schwager, P. The refined crystal structure of bovine β-trypsin at 1.8 Å resolution II. Crystallographic refinement, calcium binding site, benzamidine binding site and active site at pH 7.0. *J. Mol. Biol.* **98**, 693–717 (1975).
18. Huber, R. & Bode, W. Structural basis of the activation and action of trypsin. *Acc. Chem. Res.* **11**, 114–122 (1978).
19. Read, R. J., Brayer, G. D., Jurasek, L. & James, M. N. G. Critical evaluation of comparative model building of Streptomyces griseus trypsin. *Biochemistry* **23**, 6570–6575 (1984).
20. Blow, D. M., Birktoft, J. J. & Hartley, B. S. Role of a buried acid group in the mechanism of action of chymotrypsin. *Nature* **221**, 337–340 (1969).
21. Robertus, J. D., Kraut, J., Alden, R. A. & Birktoft, J. J. Subtilisin. Stereochemical mechanism involving transition-state stabilization. *Biochemistry* **11**, 4293–4303 (1972).
22. Ménard, R. & Storer, A. C. Oxyanion hole interactions in serine and cysteine proteases. *Biol. Chem. Hoppe Seyler* **373**, 393–400 (1992).
23. Walsh, K. A. Trypsinogens and trypsins of various species. *Methods Enzymol.* **19**, 41–63 (1970).
24. Schwert, G. W., Neurath, H., Kaufman, S. & Snoke, J. E. The specific esterase activity of trypsin. *J. Biol. Chem.* **172**, 221–239 (1948).
25. Sinn, L. G., Behrens, O. K. & Bromer, W. W. The hydrolysis of glucagon with subtilisin. *J. Am. Chem. Soc.* **79**, 2805–2807 (1957).
26. Richards, F. M. On the enzymatic activity of subtilisin-modified ribonuclease. *Proc. Natl Acad. Sci.* **44**, 162–166 (1958).
27. Harris, J. I. & Roos, P. The action of pepsin and subtilisin on β-melanocyte-stimulating hormone. *Biochem. J.* **71**, 445–451 (1959).
28. Morihara, K., Oka, T. & Tsuzuki, H. Comparison of α-chymotrypsin and subtilisin BPN': size and specificity of the active site. *Biochem. Biophys. Res. Commun.* **35**, 210–214 (1969).
29. Sun, H., Panicker, R. C. & Yao, S. Q. Activity based fingerprinting of proteases using FRET peptides. *Pept. Sci.* **88**, 141–149 (2007).
30. Chang, K. H., Auvinen, P., Hyypiä, T. & Stanway, G. The nucleotide sequence of coxsackievirus A9; implications for receptor binding and enterovirus classification. *J. Gen. Virol.* **70**, 3269–3280 (1989).
31. Chang, K. H., Day, C., Walker, J., Hyypiä, T. & Stanway, G. The nucleotide sequences of wild-type coxsackievirus A9 strains imply that an RGD motif in VP1 is functionally significant. *J. Gen. Virol.* **73**, 621–626 (1992).
32. Williams, Ç. H. et al. Integrin αvβ6 is an RGD-dependent receptor for coxsackievirus A9. *J. Virol.* **78**, 6967–6973 (2004).
33. Roivainen, M. et al. Entry of coxsackievirus A9 into host cells: specific interactions with αvβ3 integrin, the vitronectin receptor. *Virology* **203**, 357–365 (1994).
34. Triantafilou, M. et al. Involvement of β2-microglobulin and integrin αvβ3 molecules in the coxsackievirus A9 infectious cycle. *J. Gen. Virol.* **80**, 2591–2600 (1999).
35. Roivainen, M. et al. RGD-dependent entry of coxsackievirus A9 into host cells and its bypass after cleavage of VP1 protein by intestinal proteases. *J. Virol.* **65**, 4735–4740 (1991).
36. Hughes, P. J., Horsnell, C., Hyypiä, T. & Stanway, G. The coxsackievirus A9 RGD motif is not essential for virus viability. *J. Virol.* **69**, 8035–8040 (1995).
37. Ioannou, M. & Stanway, G. Tropism of coxsackie virus A9 depends on the +1 position of the RGD (arginine- glycine- aspartic acid) motif found at the C' terminus of its VP1 capsid protein. *Virus Res.* **294**, 198292 (2021).
38. Evans, R. et al. Protein complex prediction with AlphaFold-Multimer. *bioRxiv* https://doi.org/10.1101/2021.10.04.463034 (2022).
39. Jumper, J. et al. Highly accurate protein structure prediction with AlphaFold. *Nature* **596**, 583–589 (2021).
40. Oldfield, C. J. & Dunker, A. K. Intrinsically disordered proteins and intrinsically disordered protein regions. *Annu. Rev. Biochem.* **83**, 553–584 (2014).
41. Fontana, A. et al. Correlation between sites of limited proteolysis and segmental mobility in thermolysin. *Biochemistry* **25**, 1847–1851 (1986).
42. Adiyaman, R., Edmunds, N. S., Genc, A. G., Alharbi, S. M. A. & McGuffin, L. J. Improvement of protein tertiary and quaternary structure predictions using the ReFOLD refinement method and the AlphaFold2 recycling process. *Bioinform. Adv.* **3**, vbad078 (2023).
43. Zundert et al. The HADDOCK2.2 web server: user-friendly integrative modeling of biomolecular complexes. *J. Mol. Biol.* **428**, 720–725 (2016).
44. Zhou, H.-X. & Pang, X. Electrostatic interactions in protein structure, folding, binding, and condensation. *Chem. Rev.* **118**, 1691–1741 (2018).
45. Salmon, L. et al. NMR characterization of long-range order in intrinsically disordered proteins. *J. Am. Chem. Soc.* **132**, 8407–8418 (2010).
46. Parigi, G. et al. Long-range correlated dynamics in intrinsically disordered proteins. *J. Am. Chem. Soc.* **136**, 16201–16209 (2014).
47. Jackson, S. E. & Fersht, A. R. Contribution of long-range electrostatic interactions to the stabilization of the catalytic transition state of the serine protease subtilisin BPN'. *Biochemistry* **32**, 13909–13916 (1993).
48. Batra, J. et al. Long-range electrostatic complementarity governs substrate recognition by human chymotrypsin C, a key regulator of digestive enzyme activation*. *J. Biol. Chem.* **288**, 9848–9859 (2013).
49. Gandhi, P. S., Chen, Z., Mathews, F. S. & Cera, E. D. Structural identification of the pathway of long-range communication in an allosteric enzyme. *Proc. Natl Acad. Sci.* **105**, 1832–1837 (2008).
50. Zhu, J., Wang, J., Han, W. & Xu, D. Neural relational inference to learn long-range allosteric interactions in proteins from molecular dynamics simulations. *Nat. Commun.* **13**, 1661 (2022).
51. Wright, P. E. & Dyson, H. J. Linking folding and binding. *Curr. Opin. Struct. Biol.* **19**, 31–38 (2009).
52. Suskiewicz, M. J., Sussman, J. L., Silman, I. & Shaul, Y. Context-dependent resistance to proteolysis of intrinsically disordered proteins. *Protein Sci.* **20**, 1285–1297 (2011).
53. Johnson, D. E. et al. High-throughput characterization of intrinsic disorder in proteins from the protein structure initiative. *J. Struct. Biol.* **180**, 201–215 (2012).
54. Mirdita, M. et al. ColabFold: making protein folding accessible to all. *Nat. Methods* **19**, 679–682 (2022).
55. Plevka, P., Perera, R., Cardosa, J., Kuhn, R. J. & Rossmann, M. G. Crystal structure of human enterovirus 71. *Science* **336**, 1274–1274 (2012).
56. Koshland, D. E. The key–lock theory and the induced fit theory. *Angew. Chem. Int. Ed. Engl.* **33**, 2375–2378 (1995).
57. Pak, M. A. et al. Using AlphaFold to predict the impact of single mutations on protein stability and function. *PLoS ONE* **18**, e0282689 (2023).
58. Olive, M., Gan, C., Carratalà, A. & Kohn, T. Control of waterborne human viruses by indigenous bacteria and protists Is influenced by temperature, virus type, and microbial species. *Appl. Environ. Microbiol.* **86**, e01992-19 (2020).
59. Ferguson, M. & Ihrie, J. Most probable number and other microbial enumeration techniques. https://cran.r-project.org/web/packages/MPN/MPN.pdf (2019).

60. Rappsilber, J., Mann, M. & Ishihama, Y. Protocol for micro-purification, enrichment, pre-fractionation and storage of peptides for proteomics using StageTips. *Nat. Protoc.* **2**, 1896–1906 (2007).
61. Dorfer, V. et al. MS Amanda, a universal identification algorithm optimized for high accuracy tandem mass spectra. *J. Proteome Res.* **13**, 3679–3684 (2014).
62. Mirdita, M., Steinegger, M. & Söding, J. MMseqs2 desktop and local web server app for fast, interactive sequence searches. *Bioinformatics* **35**, 2856–2858 (2019).
63. Mirdita, M. et al. Uniclust databases of clustered and deeply annotated protein sequences and alignments. *Nucleic Acids Res.* **45**, D170–D176 (2017).
64. Mitchell, A. L. et al. MGnify: the microbiome analysis resource in 2020. *Nucleic Acids Res.* **48**, D570–D578 (2019).
65. Steinegger, M. et al. HH-suite3 for fast remote homology detection and deep protein annotation. *BMC Bioinforma.* **20**, 473 (2019).
66. Xue, L. C., Rodrigues, J. P., Kastritis, P. L., Bonvin, A. M. & Vangone, A. PRODIGY: a web server for predicting the binding affinity of protein–protein complexes. *Bioinformatics* **32**, 3676–3678 (2016).
67. Kuriata, A. et al. CABS-flex 2.0: a web server for fast simulations of flexibility of protein structures. *Nucleic Acids Res.* **46**, gky356 (2018).
68. Kyte, J. & Doolittle, R. F. A simple method for displaying the hydropathic character of a protein. *J. Mol. Biol.* **157**, 105–132 (1982).
69. Rodrigues, J. P. G. L. M. et al. Clustering biomolecular complexes by residue contacts similarity. *Proteins Struct. Funct. Bioinform.* **80**, 1810–1817 (2012).
70. Pettersen, E. F. et al. UCSF ChimeraX: structure visualization for researchers, educators, and developers. *Protein Sci.* **30**, 70–82 (2021).
71. Corre, M.-H. et al. Zenodo—the early communication stages between serine proteases and enterovirus capsids in the race for viral disintegration [Dataset]. Zenodo https://zenodo.org/records/12532161 (2024).

Acknowledgements

We thank EPFL collaborators for valuable discussions or technical support: L.F.K., M.D.P., M.L. We thank the Flow Cytometry Core Facility (EPFL) and M.P from the Proteomic Core Facility (EPFL) for the use of the equipment and assistance. We thank S.B. and C.S.-K. (Finnish National Institute for Health and Welfare) for providing the environmental CVA9 isolate. This research was funded by the Swiss National Science Foundation (grant no. 310003A-182468).

Author contributions

Conceptualization: M.H.C., T.K., and B.R. Methodology: M.H.C. and S.C.D. Investigation: D.C., M.H.C., S.C.D., B.R., and S.T. Visualization: M.H.C. Data curation: M.H.C. Formal analysis: M.H.C. Project administration: M.H.C. Funding acquisition: T.K. Supervision: M.H.C. and T.K. Writing—original draft: M.H.C. Writing—review & editing: M.H.C., S.C.D., and T.K. All authors read and approved the final version of the manuscript.

Competing interests

The authors declare no competing interests.

Additional information

Supplementary information The online version contains supplementary material available at https://doi.org/10.1038/s42003-024-06627-2.

Correspondence and requests for materials should be addressed to Marie-Hélène Corre.

Peer review information *Communications Biology* thanks Shailly Tomar and the other, anonymous, reviewer(s) for their contribution to the peer review of this work. Primary Handling Editors: Manidipa Banerjee and Johannes Stortz.